Chapter 2

Principle

The basic theory of near-field recording and the proposed fiber-based integrated optical pickup are discussed. Fabrication of the device is described.

2.1 Near-field recording

In near-field recording, a high numerical aperture was achieved by inserting a solid immerse lens (SIL) between the objective lens and the surface-incident disk, as shown in Fig. 2-1.

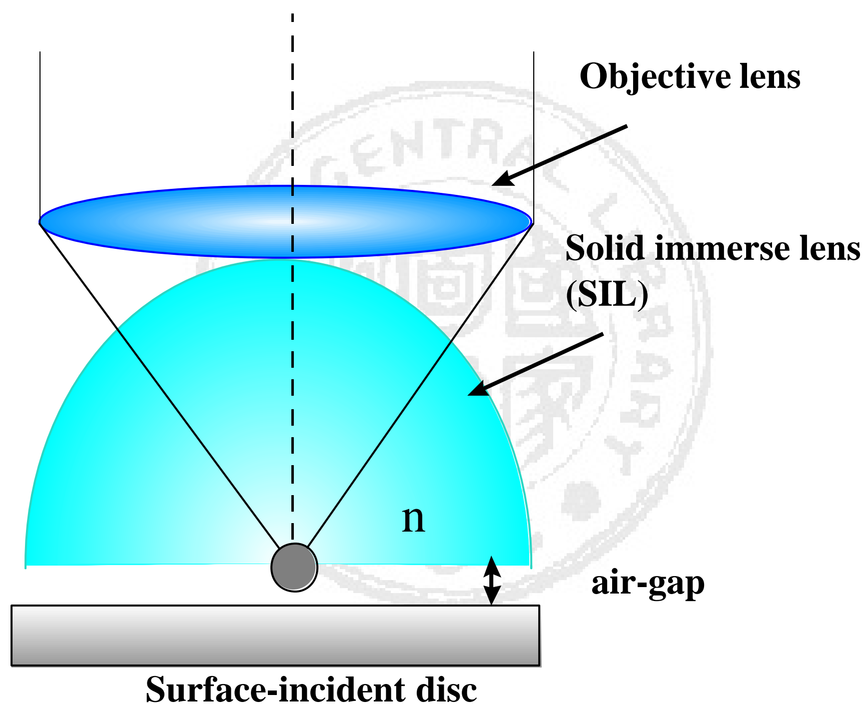

Fig. 2-1 High numerical aperture optical system in the near-field recording

Since the refractive index n of the SIL was larger than one, the wavelength of the laser beam focused by the objective lens was shortened by a factor of n. Therefore, the effective numerical aperture of the combination of the objective lens and the SIL can be increased by a factor n; thus, the laser spot size inside the SIL can also be reduced by a factor of n:

$$\text{optical spot size using SIL} \cong 0.528\frac{\lambda}{n \cdot NA} \qquad \text{(2-1)}$$
$$\text{effective NA of combined objective lens and SIL} = n \cdot NA$$

where NA denotes the numerical aperture of the objective lens. Consequently, the recording density of the surface-incident disk can be increased by a factor of n^2.

When the focused laser light propagating from the SIL with refractive index $n > 1$ into the air, the total reflection shall occur in the interface as the incident angle q_i of laser light in SIL is larger than the critical angle q_c ($q_c = sin^{-1}(1/n)$) or $n\ sin q_i > 1$ according to the Snell's law[25], as shown in Fig. 2-2. However, according to the electro-magnetic wave theorem[26], the amplitude of transmission electric field Et or the transmission light from the SIL into the air shall decay exponentially, according to Eq. (2-2):

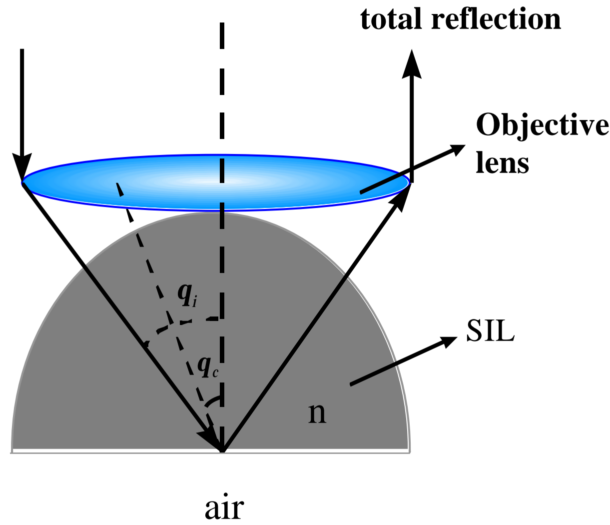

Fig. 2-2 Total reflection shall occur when the incident angle ?$_i$ of laser light is larger than the critical angle ?$_c$

$$E_t = E_0'' e^{-K_1 x} e^{i(w'' t - k_y'' y)}$$
$$K_1 = -i\frac{w}{c}\sqrt{\left(1 - n^2 \sin^2 q_i\right)} \quad (2\text{-}2)$$

where $1/K_1$ is defined as the skin depth. Therefore, the transmission light wave or electric field E_t can still extend a distance of skin depth from the SIL surface at $q_i > q_c$, as shown in Fig. 2-3. Therefore, the transmission light wave E_t was called evanescent wave or surface wave. When the surface-incident disk is placed near the SIL surface within the skin depth, the evanescent light wave can be coupled into the surface-incident thin-film layers, as shown in Fig. 2-4.

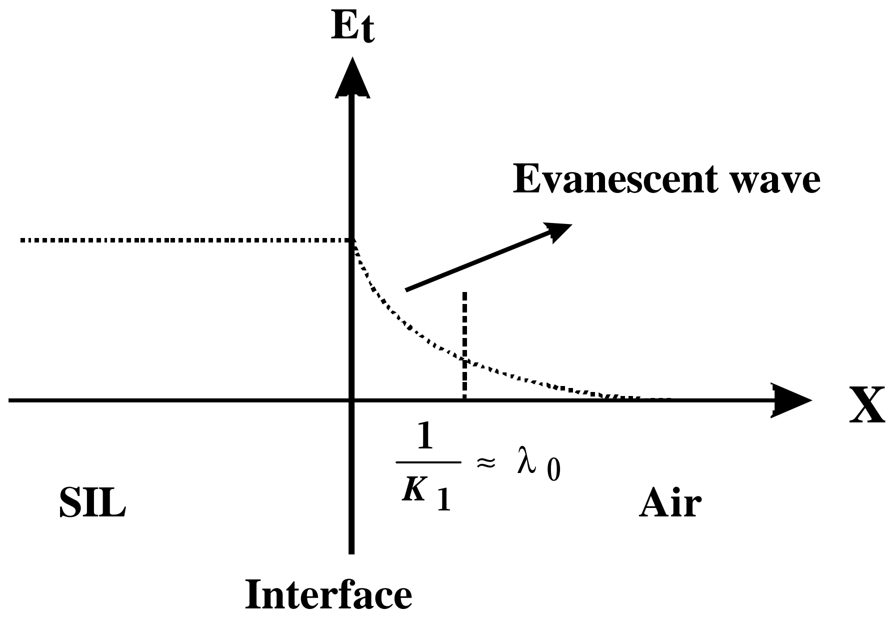

Fig. 2-3 Evanescent wave exists only within the skin depth from the surface of SIL

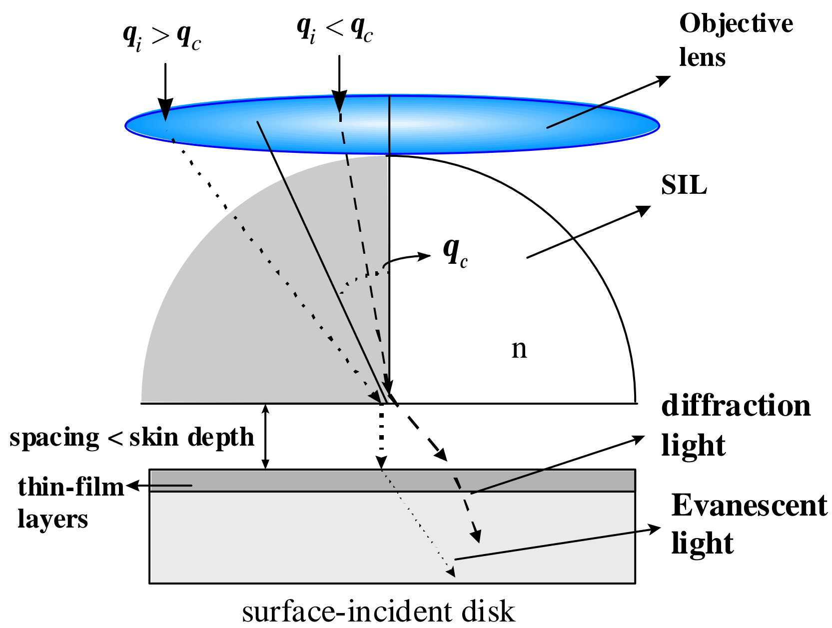

Fig. 2-4 Refractive (?$_i$ <?$_c$) and evanescent (?$_i$ > ?$_c$) light in the surface-incident disk

The incident laser light in the SIL with $?_i < ?_c$ shall refract into the surface-incident disk according to the Snell' s law, while the incident light with $?_i > ?_c$ shall couple into the disk thin-film layers by means of the evanescent wave. Combined the refractive light ($?_i < ?_c$) and sufficient coupled evanescent light ($?_i > ?_c$), the spot size formed in the surface-incident disk can achieve almost the same small size as the diffraction-limited spot formed inside the SIL. For increasing the recording density by a sufficient small spot size, a high effective numerical aperture of the combination of an objective lens and an SIL is necessary and can be achieved by increasing the objective NA and the refractive index n of the SIL according to Eq. (2.1). However, the skin depth $1/K_1$ decreases as the high effective numerical aperture increases. Usually, the skin depth is in the order of several tenths wavelength. To transfer the small spot size effectively from the SIL into the recording layer of the optical disk for high density recording, the surface-incident disk structure was adopted, as shown in Fig. 2-5. In addition, the surface-incident disk has to be very close to the SIL to couple sufficient evanescent light energy for maintaining the small spot size transferring from the SIL into the recording layer.

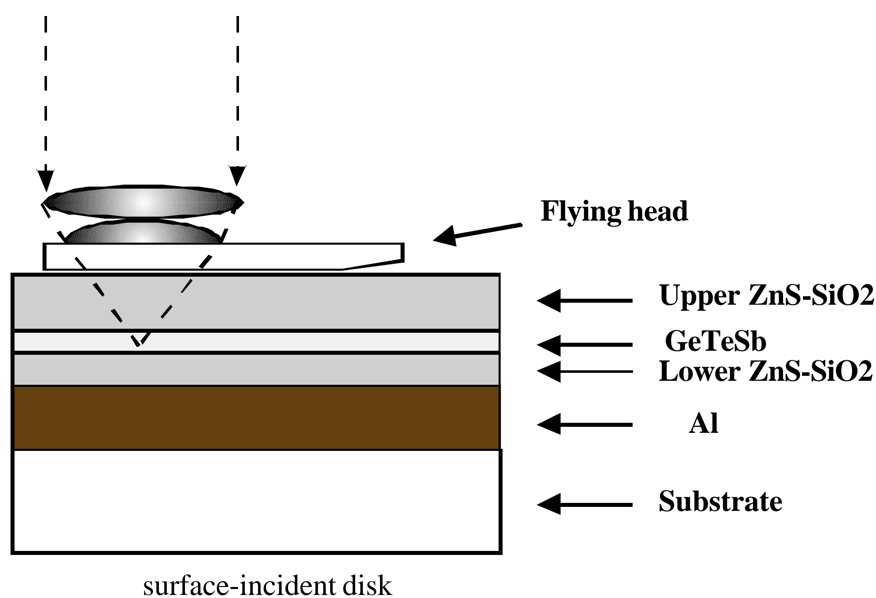

Fig. 2-5 Surface-incident disk structure

2.2 Solid immersion lens (SIL) system

Solid Immersion Lens (SIL) systems are attractive because they produce spots smaller than conventional optical systems with high throughput to the recording layer. The areal density achievable with conventional optical recording technology is determined by the diffraction limit. The minimum focused spot diameter (full-width at $1/e^2$) is approximately λ/NA_{EFF}, where λ is the free space wavelength and $NA_{EFF} = n\sin\theta$ (n is the refractive index of the image space, and θ is the marginal ray angle). Typically, the NA_{EFF} is ~ 0.5 in air and the minimum diameter of the optical spot is in the order of λ.

The diffraction limit can be circumvented by the use of near-field optics. In 1984 Pohl *et al*[27]. demonstrated a near-field optical microscope using a glass rod tapered down to a small pinhole and covered it with a deposited metal film. To obtain a resolution comparable to the diameter of the pinhole, the pinhole must be placed from the sample within a distance comparable to the pinhole size. Betzig *et al.*[28] used a taped fiber with a pinhole at the end to demonstrate a resolution of 60 nm with a 488 nm light source. Hosaka and others[29] utilized near-field optics to record in phase-change (PC) media and achieved a minimum recorded mark of 60 nm with a 785 nm laser. One major issue of using these tapered fibers is the high transmission loss of the light; (throughput is approximately 10^{-3}~10^{-4} with the aperture diameter of 100 nm[30]).

An alternative approach with solid immersion lens (SIL) proposed by Kino *et al*[31].provided a scanning image directly, required no mechanical scanning, had a higher light budget, and could be easily added onto an existing optical data storage

system. Therefore, SIL-based optical systems are more feasible than other near-field techniques in the high-data-rate optical storage applications[32].

A typical solid immersion lens (SIL) system shown in Fig. 2-6 includes an objective lens and an SIL which is nearly in contact with the sample. The incident light is focused with a marginal angle θ at the hemispherical center of a high-refractive-index SIL without refraction. The NA_{EFF} of the system is increased by a factor n, where n is the refractive index of the SIL. Therefore, the focused spot size becomes smaller and the mark density becomes higher.

In the case of $NA_{EFF} > 1.0$, this setup becomes a near-field approach. The outer rays exceeding the critical angle ($\theta_c = \sin^{-1} 1/n$) are totally internally reflected at the air/SIL interface and the field associated with them falls off exponentially away from the interface. This will degrade both the focused spot and the reflected signal.

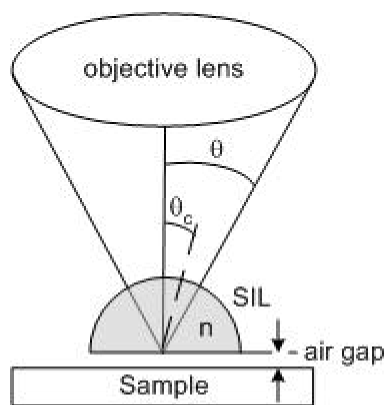

Fig. 2-6 Hemispherical SIL focusing at the bottom surface.

The SIL-based system is often used when the sample is placed within 100 nm from the SIL with visible light. For example, the 1/e decay distance $d_{1/e}$ of the evanescent energy at NA_{EFF} is given by[33]:

$$d_{1/e} = \frac{\lambda}{4\pi} \frac{1}{\sqrt{NA_{EFF} - 1}} \tag{2-3}$$

For $\lambda = 650$ nm and $NA_{EFF} = 1.2$, $d_{1/e} \cong 115$ nm.

Further improvement can be achieved by using a stigmatic focusing lens, as illustrated in Fig. 2-7 (a). In this case, the converging cone of light aimed at a distance $n \times a$ below the center of a sphere (with radius a and refractive index n) will focus a diffraction-limited spot at the distance a/n below the sphere center after the refraction, and the NA_{EFF} can be increased by a factor of n^2, not only because the wavelength within the super SIL is shortened by a factor n, but also the sine of the cone angle, $\sin\theta$, is increased by a factor of n. However, the full factor of n^2 mentioned above cannot be realized without any limitation since the bending of the marginal ray within SIL cannot exceed 90°, as shown in Fig. 2-7 (b). The super SIL can only increase its $\sin\theta$ up to 1, at which the remaining rays will miss the super SIL. Thus this limits the NA of the objective lens to 1/n and the maximum NA_{EFF} of the super SIL system is nNA, and not n^2NA.

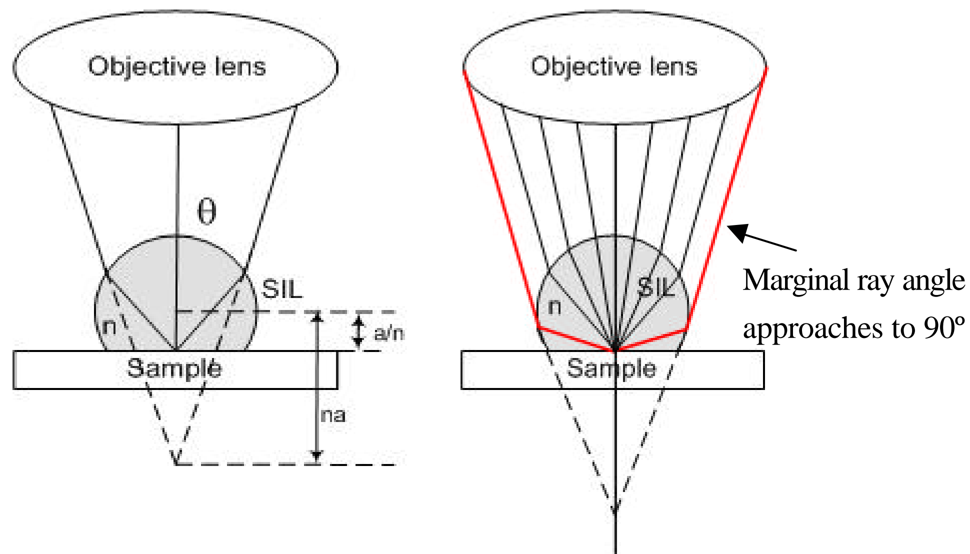

Fig. 2-7 (a) Super SIL. (b) The marginal ray angle approaches 90° with respect to the image space.

2.3 Fiber-based integrated optical pickup

The integrated optical pickup can be modified by separating the waveguide chip and the laser diode (LD), and linking them with an optical fiber. In the fiber-based pickup, only the waveguide chip is actuated for servo operation. The reduction in weight of the moving part allows higher speed operation. Another advantage of the fiber-based pickup is that an optical isolator can be easily inserted between the LD and the fiber to stabilize the laser operation. In our approach, a microlens formed on the end of a single-mode fiber (SMF) is used to replace the traditional objective lens. This fiberlens is designed to overcome the tight tolerances found in the high NA optical path and to reduce the number of components, thus the cost and weight of the head. To further realize a smaller spot size, the optical fiber is combined with a well-defined mechanical structure including a solid immersion lens (SIL) and a sub-micrometer aperture, as shown in Fig. 2-8. In this scheme, light is guided by the core of a single-mode fiber and focused through microlens on the bottom of the SIL-aperture combination.

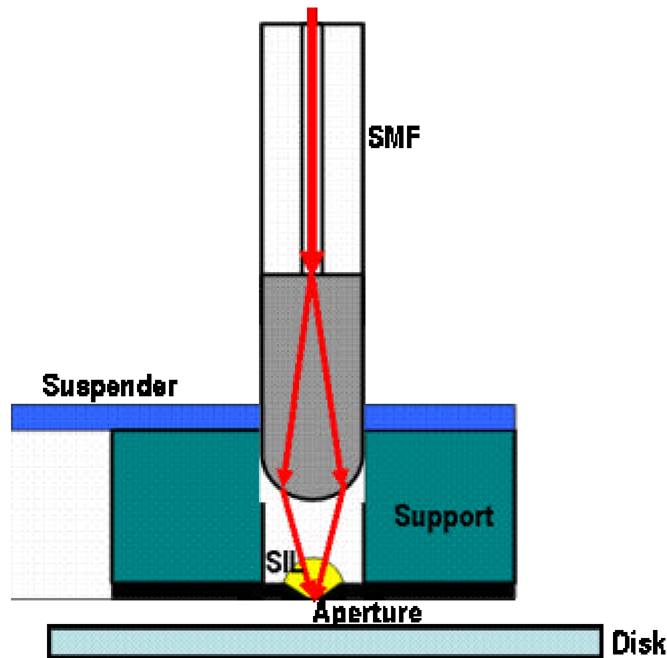

Fig. 2-8 Schematic of the integrated optical disk pickup (IODPU) that integrates a fiberlens, SIL and sub-micrometer aperture.

The schematic of the SIL/aperture/support combination is shown in Fig. 2-9. The fabrication process involves photolithography, electroplating, and thermal reflow. Detailed description can be found in Reference [34].

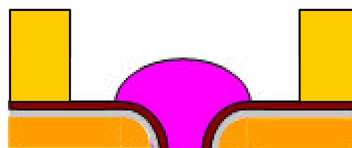

Fig. 2-9 Schematic of SIL/aperture/support combination

2.4 Planar integrated optical pickup

Since bending fiber into a sharp angle causes damage, the vertical integrated pickup structure shown in Fig. 2-8 is not compact. Moreover, the thickness of the support has to be sufficient to fix the fiber (~1 mm). The high aspect ratio of this structure, 125 μm in diameter and 1 mm in height, is difficult to achieve by photolithography. Thus, a planar integrated head structure that combines an optical fiber, a SIL, a planar coil and a GMR (Giant Magnetic Resist) by MOEMs technology was proposed, as shown in Fig. 2-10[35]. This device is planar and can be mounted on a slider and suspension like the magnetic flying head used in HDD system.

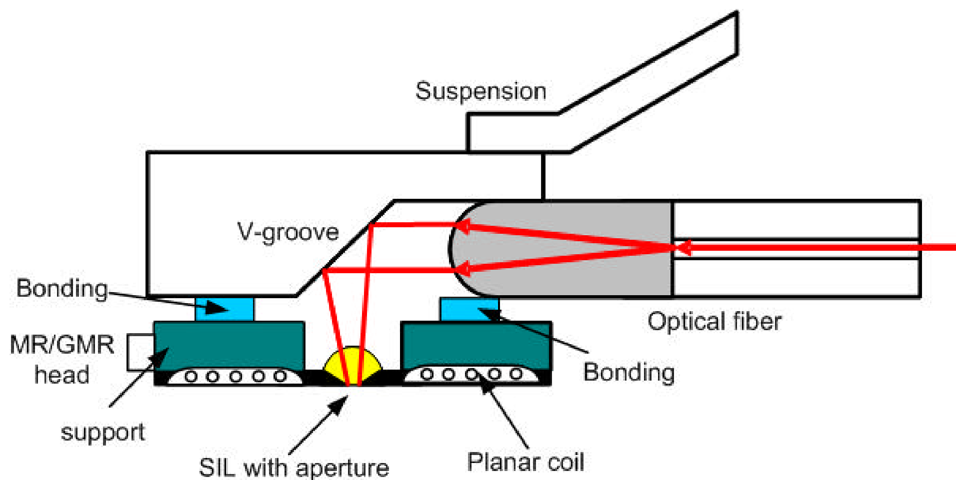

Fig. 2-10 Schematic of the proposed planar integrated pickup

The light is guided into the optical fiber fixed in the well defined V-groove. The beam is collimated and shaped by the front-end fiberlens. The optical path was turned by a 45 °mirror. The beam size is further reduced by the SIL and the aperture. The V-groove and the 45 °mirror can be realized by silicon bulk micromaching.

2.5 Si bulk micromaching

Wet anisotropic chemical etching of silicon is one of the key technologies in silicon micromachining. The simplest and most widely used micromachined structure for fiber applications is an anisotropically etched V-groove on a (100) silicon wafer. The groove is defined by {111} planes that are slanted at 54.7 °to the surface. The side walls of the groove can act as mirrors. There are applications where a 45 °mirror plane at the end of the groove is needed to provide a right angle change for the light path. Because of the precise orientation between different crystal planes, anisotropic etching can be used to fabricate precise three dimensional structures such as 45° mirror on the (110)-planes. Wet chemical etching in pure KOH (potassium hydroxide), EDP (ethylene diamine-pyrocatechol), TMAH (tetramethy ammonium hydroxide), N_2H_4 (hydrazine), or KOH with isopropyl alcohol (KOH/IPA) is known to etch different crystal planes at different etching rates. The main reaction equations for all the mentioned etchants are described as following:

1. Silicon atoms act with OH^- on the surface

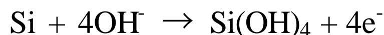

$Si + 4OH^- \rightarrow Si(OH)_4 + 4e^-$

2. $Si(OH)_4$ in step 1. dissolves in the solution when pH ＞ 12

$Si(OH)_4 \rightarrow SiO_2(OH)_2^{2-} + 2H^+$

$2H^+ + 2OH^- \rightarrow 2H_2O$

3. Four e^- in step 1. act with H_2O

$4H_2O + 4e^- \rightarrow 4H_2O^-$

$4H_2O^- \rightarrow 4OH^- + 2H_2$

described above, OH^- and H_2O are the main substance in the reactions. The other additives, such as pyrazine or 2-propanol (IPA), will cause the change in etching rate.

Most of the reported anisotropic etchants are aqueous alkaline solutions, either organic or inorganic. Among them the most widely used is KOH. The anisotropy is strongly dependent on the etchant composition, etchant concentration, dopant concentration, temperature and even stirring. Because the smoothness of the etched surface can be improved by adding IPA to pure KOH solution, the KOH/IPA etchant is used to fabricate the (110)-groove with sidewalls at 45 °angles to the surface of the (100)-oriented silicon substrate.

Crystalline silicon forms a covalently bonded structure, the diamond-cubic structure, which has the same atomic arrangement as carbon in diamond form and belongs to the more general zinc-blend classification. Silicon, with its four covalent bonds, coordinates itself tetrahedrally, and these tetrahedrons make up the diamond-cubic structure. This structure can also be represented as two interpenetrating face-centered cubic lattices, one displaced (1/4, 1/4, 1/4)a with respect to the other, as shown in Fig. 2-11.

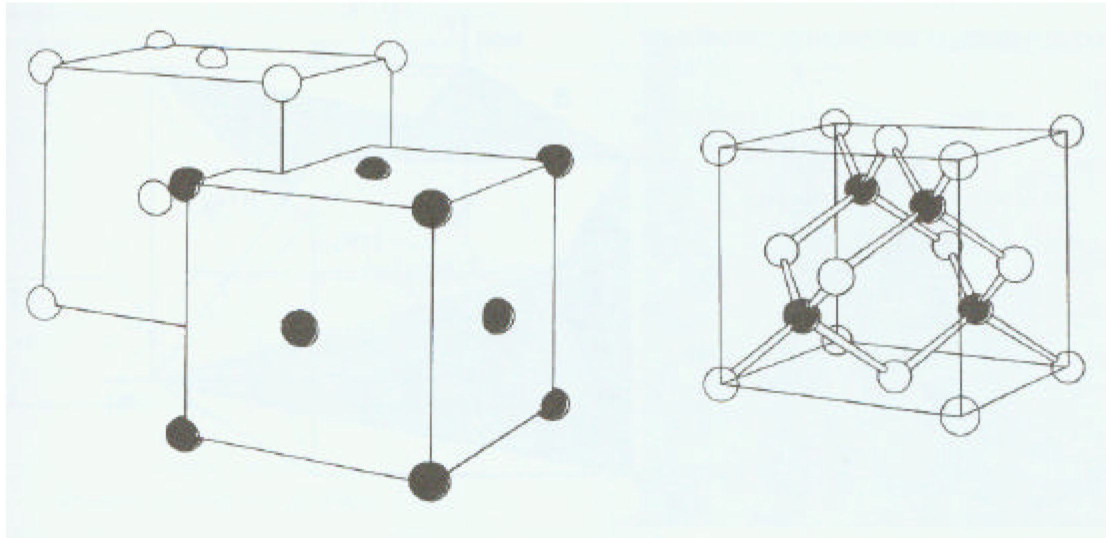

Fig. 2-11 The diamond-type lattice can be constructed from two interpenetrating face-centered cubic unit cells. Si forms four covalent bonds, making tetrahedrons.

For such a cubic lattice, direction [hkl] is perpendicular to a plane with the Miller indices (hkl). The lattice parameter 'a' for silicon is 5.4309Å. Its diamond-cubic lattice is surprisingly wide open, with a packing density of 34%, compare to 74% for a regular face-centered cubic lattice. The {111} planes present the highest packing density and the atoms are oriented such that three bonds are below the plane. {111} planes always have lowest etching rate for all the etchants because of its highest packing density.

In Fig. 2-12, the unity cell of a silicon lattice is shown together with the correct orientation of a [100]-type wafer relative to this cell. It can be seen from this figure that intersections of the nonetching {111} planes with the {100} planes are mutually perpendicular and lying along the <110> orientations. Provided a mask opening (a rectangular or a square) is accurately aligned with the primary orientation flat, i.e., the [110] direction, only {111} planes will be introduced as sidewalls from the very beginning of etching, as shown in Fig. 2-13 (a).

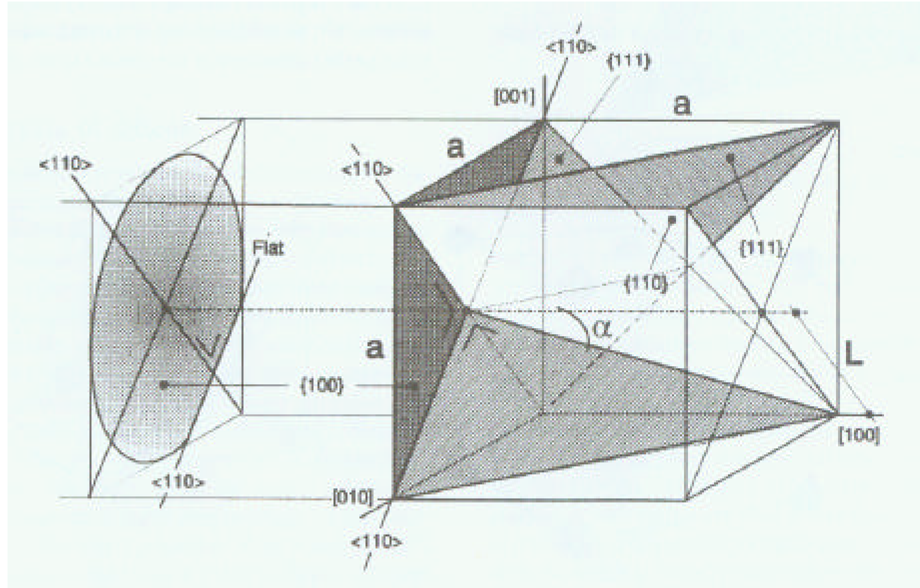

Fig. 2-12 (100) silicon wafer with reference to the unity cube and its relevant planes

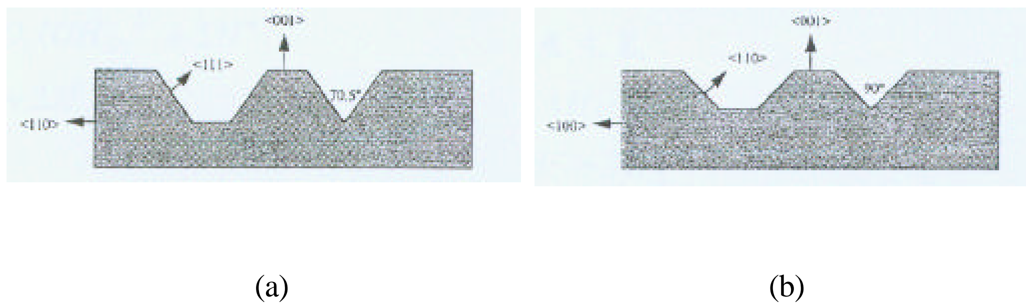

(a) (b)

Fig. 2-13 (a) V-groove formed by the mask opened parallel to (110)-flat

(b) 90 °V-groove formed by the mask opened parallel to (100)-flat

By aligning the mask accurately with the (010)-flat, i.e., 45 ° to (110) primary orientation flat, and choosing the anisotropic etchant with a selectivity of (100)/(110) > 1, a 90 °V-groove bounded by (110) sidewalls can be obtained, as shown in Fig. 2-13 (b). Furthermore, the (110)-plane can be used as a 45 °mirror for its orientation on (100) wafer and its smoothness.